AFRL-AFOSR-UK-TR-2021-0023

Liquid crystal light valves driven by photovoltaic fields: Continuation

Alexander Lorenz
Universitat Paderborn
Warburger Str. 100
Warburger Str. 100, , 33098
DE

08/02/2021
Final Technical Report

Air Force Research Laboratory
Air Force Office of Scientific Research
European Office of Aerospace Research and Development
Unit 4515 Box 14, APO AE 09421

REPORT DOCUMENTATION PAGE

Form Approved
OMB No. 0704-0188

1. REPORT DATE *(DD-MM-YYYY)*	**2. REPORT TYPE**	**3. DATES COVERED** *(From - To)*
02-08-2021	Final	15 Aug 2018 - 14 Aug 2019

4. TITLE AND SUBTITLE
Liquid crystal light valves driven by photovoltaic fields: Continuation

5a. CONTRACT NUMBER

5b. GRANT NUMBER
FA9550-18-1-7002

5c. PROGRAM ELEMENT NUMBER
61102F

6. AUTHOR(S)
Alexander Lorenz

5d. PROJECT NUMBER

5e. TASK NUMBER

5f. WORK UNIT NUMBER

7. PERFORMING ORGANIZATION NAME(S) AND ADDRESS(ES)
Universitat Paderborn
Warburger Str. 100
Warburger Str. 100, 33098
DE

8. PERFORMING ORGANIZATION REPORT NUMBER

9. SPONSORING/MONITORING AGENCY NAME(S) AND ADDRESS(ES)
EOARD
UNIT 4515
APO AE 09421-4515

10. SPONSOR/MONITOR'S ACRONYM(S)
AFRL/AFOSR IOE

11. SPONSOR/MONITOR'S REPORT NUMBER(S)
AFRL-AFOSR-UK-TR-2021-0023

12. DISTRIBUTION/AVAILABILITY STATEMENT
A Distribution Unlimited: PB Public Release

13. SUPPLEMENTARY NOTES

14. ABSTRACT
The results are promising to create reconfigurable diffractive samples and holograms in a thin layer of liquid crystal via the controlled exposure to light. The control of laser generated defects is essential for this purpose and this goal has been achieved, successfully. The ongoing work now focuses on control of the writing setup (movable sample vs. scannable beam) and improved exposure quality. In addition, Light valving (quickly redirecting light) was investigated in samples where the optical axis of the substrates was in plane and the optical axis of a nematic LC was (initially) aligned perpendicular. These samples could be switched from a dark state to a transmissive state, efficiently. The field induced (light induced) director reorientation was understood in detail.

15. SUBJECT TERMS

16. SECURITY CLASSIFICATION OF:			**17. LIMITATION OF ABSTRACT**	**18. NUMBER OF PAGES**	**19a. NAME OF RESPONSIBLE PERSON**
a. REPORT	**b. ABSTRACT**	**c. THIS PAGE**			NATHANIEL LOCKWOOD
U	U	U	SAR	20	**19b. TELEPHONE NUMBER** *(Include area code)* 314-235-6005

Final Performance Report

Grant Number:	FA9550-18-1-7002, complete project
Research Title:	*Liquid crystal light valves driven by photovoltaic fields: Continuation*
Principal Investigator:	Dr. rer. nat. Alexander Lorenz (until June 30th 2020), coauthor of report: Dr. Gaby Nordendorf Department of Chemistry Paderborn University Warburger Str. 100 33098 Paderborn Germany Cell phone: +49 177 305 13 24 Phone: +49 5251 60 5728 Office: NW 1 872 Web: http://chemie.uni-paderborn.de/arbeitskreise/physikalische-chemie/lorenz-a/
Period of Performance:	08/15/2018 – 08/14/2020

Abstract/Introduction: The results obtained in the first project period were promising to approach the work plan intended for the second project period, which was aimed to write patterns in hybridized LC test cells and use these as diffractive optical elements to control transmitted light. In particular, the observations from the first project period were indicating that the nature of the defects observed would require more attention: Both the type of defects seen and also the interaction of substrate and liquid crystal (promoted via photovoltaic fields) turned out to have partially unexpected and exciting features. Preliminary observations (first project period) of samples suitable for optically stimulated optical vortex generation could be completed successfully. It was found umbilical defects could be created in samples filled with a nematic liquid crystal upon exposure with a continuous wave focused laser beam (visible light). One important condition was that these samples were made with an ITO-coated covering substrate. These exciting experimental observations were explained successfully by making use of the well-known theoretical model of umbilical defects and considering the field distribution of the photovoltaic fields generated in the samples. A new and exciting type of defect was thus seen in the studied samples, which could be used to control the properties of transmitted light: A circularly polarized input beam was on purpose converted to a vortex beam. The position of optical vortices could be controlled (moved to any wanted position in the sample plane) by steering the position of the exposure beam. In order to approach writing diffractive elements based for example on stripe patterns in samples with chiral nematic LCs, the size of the defects were of interest. In the first project period, a method to get perfect circular defects and otherwise maintain a clean (defect-free) background in such samples was well understood. In the new experimental setup, the conditioning of the laser beam was perfected (fixed focus) and the sample were moved with an xy-microscope table, which was preferable to approach writing high quality patters. Already in the first experimental test series, it became clear, that there was more to the samples than had been expected. Now it became clear that systematic differences in the defects seen were caused by the nature of the substrates and not by deviations of a light distribution of a steered laser beam. The size and shape of the defects were influenced by the pretreatment conditions (were the samples exposed before?) and the substrate surface used to control the liquid crystal (had the liquid crystal been placed on the $+c$ or $-c$ surface of the z-cut iron doped lithium niobate substrates). Variations in the surface energy of the substrates were therefore investigated with control liquids.

Photo generating substrates (iron doped lithium niobate) were covered with a responsive layer of a chiral nematic liquid crystal. The devices were covered with an indium tin oxide coated glass plate, on purpose coated with polyvinyl alcohol alignment layers. The coating procedure and the pitch length of the chiral nematic liquid crystal were systematically varied in order to create perfect (without defects in the LC) samples. These samples were studied in detail. Exposure to a tightly focused laser beam resulted in circular, spot-like defects in a background

e-mail: alexander.lorenz@online.ms · cell phone: +49 177 305 13 24

of well-oriented chiral nematic LC in the uniformly standing helix configuration. The results are promising to create reconfigurable diffractive samples and holograms in a thin layer of liquid crystal via the controlled exposure to light. The control of defects is essential for this purpose and this goal has been achieved, successfully. The ongoing work now focuses on control of the writing setup (movable sample vs. scannable beam) and improved exposure quality.

Light valving was investigated in samples where the optical axis of the substrates was in-plane and the optical axis of a nematic LC was (initially) aligned perpendicular. These samples could be switched from a dark state to a transmissive state, efficiently. The field induced (light induced) director reorientation was understood in detail.

Table of Contents

e-mail: alexander.lorenz@online.ms · cell phone: +49 177 305 13 24

1. Exposure setup and imaging

As in the initial project, the samples were investigated with an inhouse assembled exposure setup (Fig. 1). We are currently testing an advanced setup with an alternative lens system to condition the laser beam, improved image quality, and a movable sample holder (piezo driven sample holder). Some sample images are included in the report (Ongoing work).

This setup used for the investigations reported was realized by modifying an inverted polarized optical microscope with additional optics: The microscope was fitted with a light emitting diode (LED) white light illumination (linearly polarized illumination, transmitted light), a removable edgepass filter and a suitable digital photo/video camera (observation of the image plane and recording of images). A diode laser (532 nm, 4.5 mW) was coupled to the microscope beam path. Beam steering (with micron precision) was realized with a precision tiling laser mount. This diode laser source had a small form factor and in a straight-forward approach, the whole unit was tilted (Fig. 2) with the laser mount. The laser beam was focused in the imaging plane by using a lens with 10 cm focal length. The beam focus was investigated with a laser beam profiler. The tilting laser mount was driven with stepper motors and controlled with a LabVIEW program. The LabVIEW program was programmed on purpose and enables both scanning in predefined trajectories and scan-to-click, where the laser beam focus could be freely positioned in the xy-plane with micron accuracy.

The edgepass filter was used to exclude any laser light from the image plane (but not from the sample plane). Hence, the transmitted white light (except the filtered wavelength range) could still be used to record images of the samples. The laser power was attenuated with a set of neutral density filters to conduct adjustments of the optics and systematic experiments with controlled laser power.

A schematic of a hybridized sample is shown (Fig. 3). Here, a LC layer was assembled in-between a photovoltaic iron doped lithium niobate (Fe:LN) substrate and a cover glass. These test cells had a cell gap of $\approx 30\ \mu$m (measured with a precision micrometer with electronic out-read).

The cover glasses were cleansed and could be treated with a polyvinyl alcohol solution (followed by thermal annealing). Samples with chiral nematic liquid crystals were investigated. Chiral nematic liquid crystals are self-assembled, soft photonic crystals and show selective reflection of light (colored samples). The properties of the chiral nematic liquid crystal and the samples investigated are comprehensively reviewed in the attached paper [1].

The results obtained in samples of a conventional nematic LC (vertically aligned) and samples with *x*-cut lithium niobate substrate (optical axis in-plane) are summarized in the attached paper [2].

e-mail: alexander.lorenz@online.ms · cell phone: +49 177 305 13 24

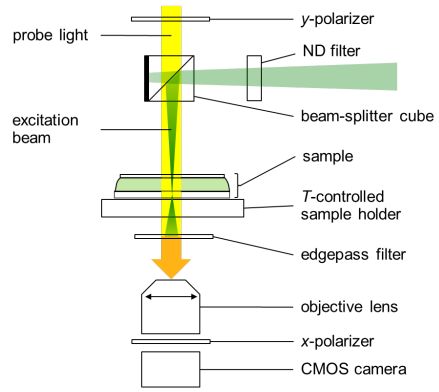

Fig. 1. Schematic of exposure setup.

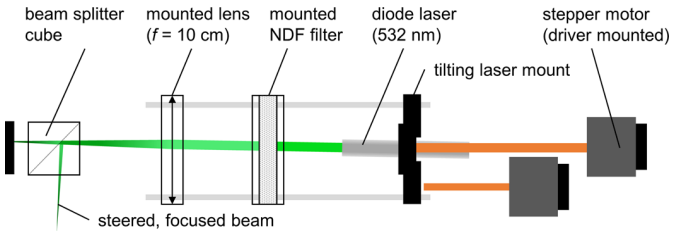

Fig. 2. Schematic of beam steering assembly.

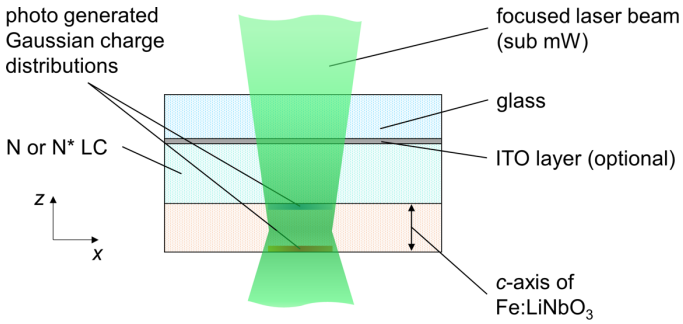

Fig. 3. Schematic (not to scale) of a test cell where a 30 μm thick LC layer was sandwiched between a Fe:LN substrate and a glass plate exposed with a focused laser beam.

2. *Control of defects in chiral nematic LCs*

2.1. Avoiding oily-streak defects and control of the defect edge

The experimental work and some theoretical considerations are comprehensively described in the attached paper [1] (published in Liquid Crystals, impact factor >3). A thermally annealed alignment layer, deposited at the covering glass, was found to reduce the surface roughness (investigated with atomic force microscopy) of the samples, reasonably. Nucleation cores for line defects, which need be avoided, were successfully suppressed and liquid crystal alignment of extraordinary high-quality was found in these samples. The chiral dopant R5011 was used to induce chirality in the LC and a concentration of 1.75 % R5011 led to the circular spots in a perfect background, as was searched for (Fig. 4).

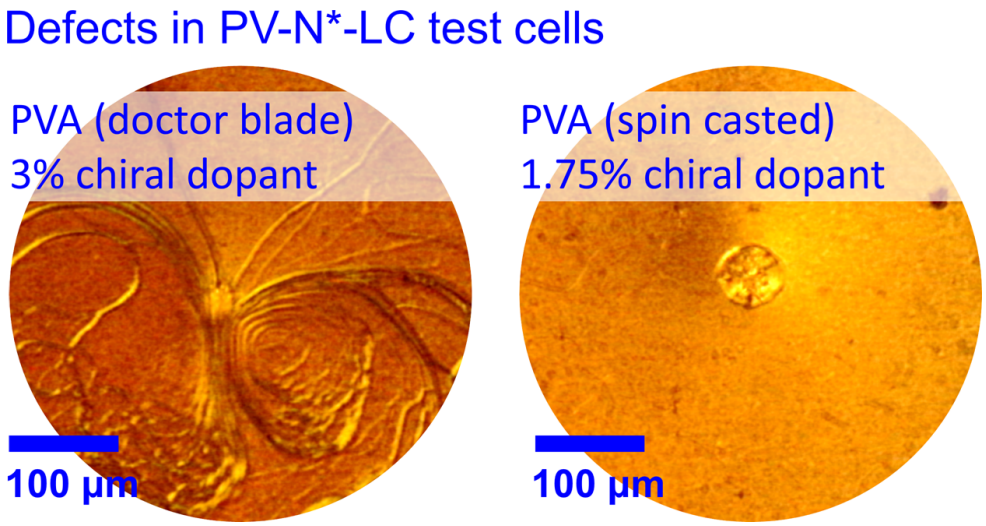

Fig. 4. Summary of the experimental work performed in chiral nematic liquid crystals. TOC image of attached paper [1].

2.2. Impact of the focusing lens

Two types of focusing lenses were studied, a lens with a focal width of 8 cm and lens with a focal width of 10 cm. Not all results were ideal, and samples exposed to a beam focused with a lens of 8 cm focal width sometimes showed more distorted defects. It is not yet fully understood, if this was caused by the slightly higher power density in these samples or slight, technical deviations in the experimental setup. However, some samples were very instructive and even smaller defects (higher resolution of the writing process) could be inscribed with the 8 cm lens as compared to the results with the 10 cm lens (Fig. 5).

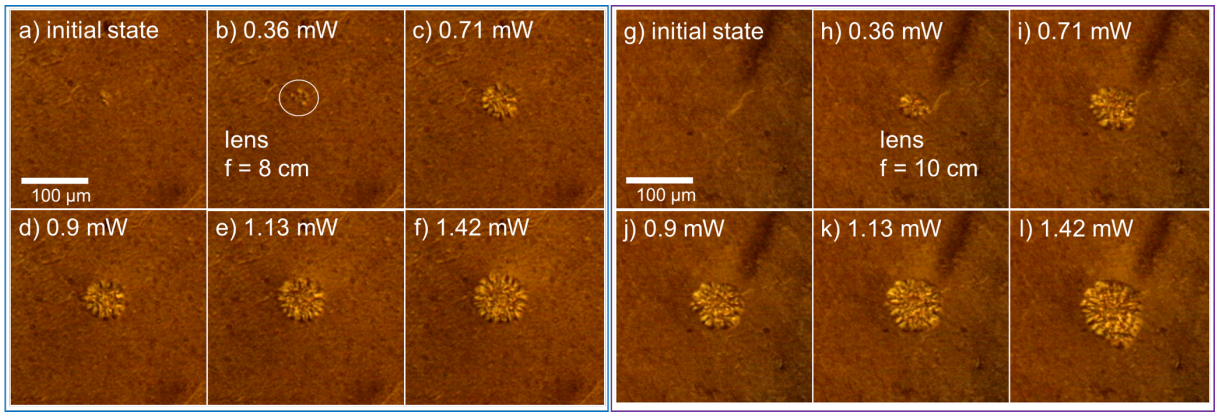

Fig. 5. Comparison of samples (with cleansed, ITO coated covering glass, chiral nematic LC, 1.75% doping concentration) exposed to a laser beam focused with a lens of 8 cm focal width (a – f) and focused with a lens of 10 cm focal width.

3. Light valving in x-cut substrates

The light induced electric field distribution on the surface of *x*-cut substrates iron doped lithium niobate substrate is schematically shown in Fig. 6. The field induced pattern, which occurred in the samples upon exposure to a focused laser beam is shown in Fig. 7. The liquid crystal director distribution is indicated. The response was fully reversible. More details along with a discussion of the required intensity (comparison to non-liner optical responses in a neat nematic liquid crystal) is given in the attached paper [2].

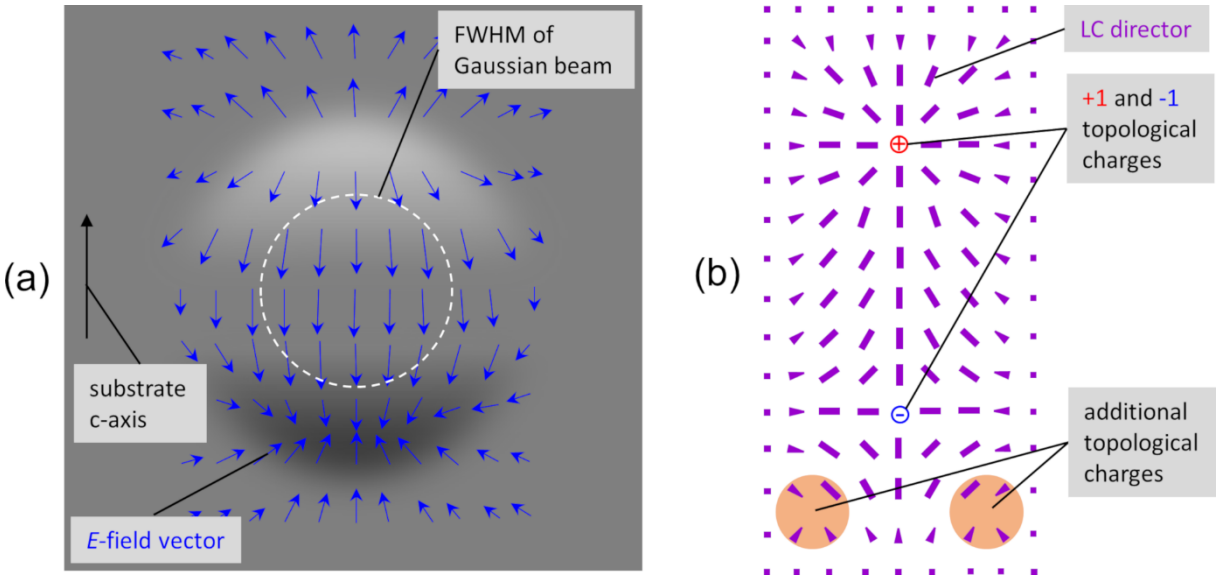

Fig. 6. (a) Schematic of photovoltaic field distribution (fields in an isotropic medium) at the surface of an *x*-cut Fe:$LiNbO_3$-substrate exposed to a Gaussian laser beam. The field amplitude is shown as shaded area (gray: zero field). (b) Composed LC director pattern, where a pair of field induced topological charges was placed in an initially homeotropic director field (wedges indicate a tilted director). In the area near the negative topological charge, formation of additional topological charges(indicated) cannot be avoided, which violates the requirement of a topologically neutral director field.

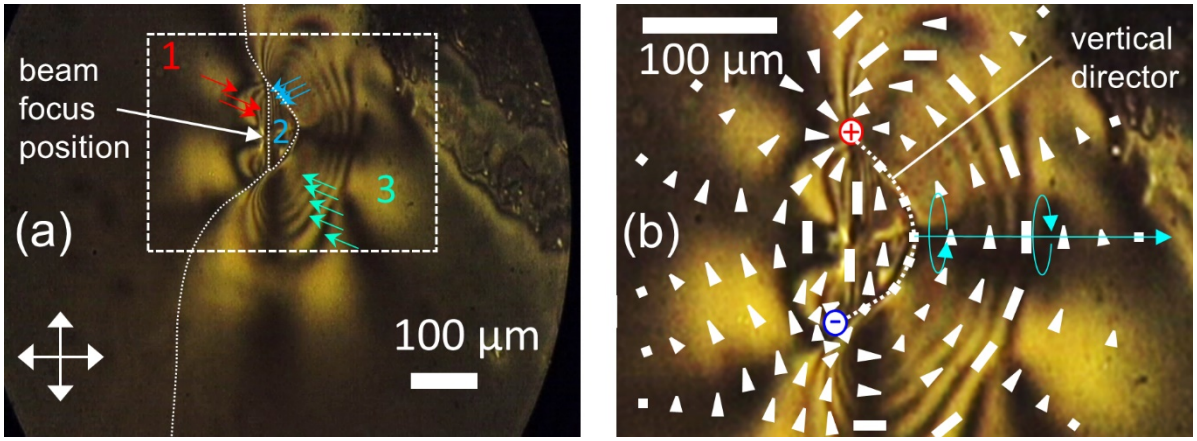

Fig. 7. (a) Observed defect pattern. Image divided in three sections by a dashed line. Birefringent stripes (dark ones) were highlighted with arrows. (b) Magnification with added schematic of director field pattern (wedges indicate out of plane tilt of the LC director).

e-mail: alexander.lorenz@online.ms · cell phone: +49 177 305 13 24

4. Work started but not finalized in project period 1

A new setup (Fig. 8) is being tested. Here, the samples are exposed through a beam splitter, which is fixed in cage optics. The setup has several advantages: The coupled laser beam can be adjusted and calibrated more efficiently. Samples can be placed on the sample holder without removing the beam splitter. The sample holder is fixed on a 3-axis positioning stage, two axes are controlled with piezo actuators: By moving the sample, patterning can be achieved with higher precision than has been possible in the previous experiments. Additional holographic beam splitters aiming for multiple-spot exposure can be mounted more easily than in previous attempts.

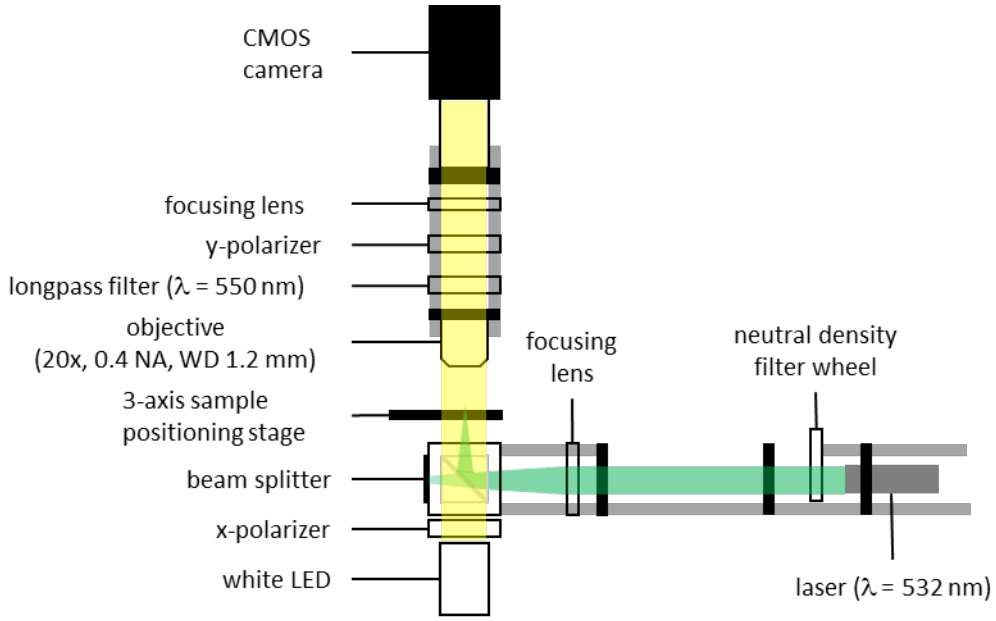

Fig. 8. Schematic of new optical setup.

Currently, the setup is being calibrated and test samples are being studied. The preliminary results obtained already show that the setup is promising to realize the research anticipated in the current project period (option 1). The image quality of the recorded images is very high. With parallel polarizers, it was seen that the defect degrades in an interesting way, if the laser shutter was closed: Tiny line defects were seen (Fig. 9a). The crystalographic *c*-axis of the field generating substrates has a direction. We were surprised that this direction has an impact on our samples. We have studied samples made with the same substrate. A nematic liquid crystal was placed on the substrate, spacer film was placed on the samples, and the sample was covered with a cleansed glass plate. The sample was investigated, the substrate was cleaned and then the liquid crystal along with spacer films and covering glass was placed on the other side of the substrate. Surprisingly, the light induced defects seen had a different appearance (Fig. 9b and c). The results are promising and samples with different direction (positive or negative) of the crystallographic *c*-axis are now studied in more detail.

e-mail: alexander.lorenz@online.ms · cell phone: +49 177 305 13 24

(a) 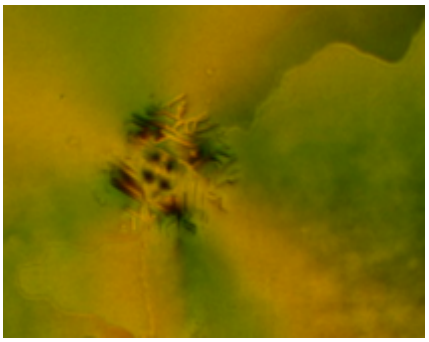 (b) 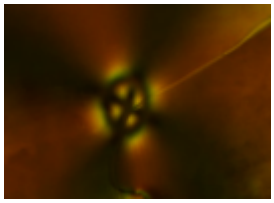 (c) 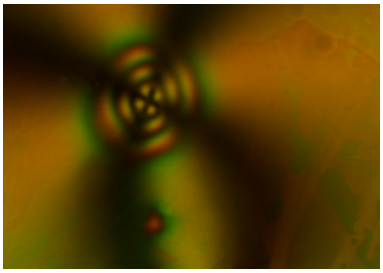

Fig. 9. Images recorded in samples studied with the new optical setup. (a) Wrinkle like texture in samples after the laser beam shutter has just been closed. (b) Defect (one dark ring) seen in sample with z-cut substrate. (c) Defect with 3 dark rings seen in a sample made with the same substrate as in (b), at the same exposure intensity, but assemble with reversed substrate.

5. Studying a new type of light induced umbilical defects

The properties of umbilical defects are fascinating, and they have obtained a great deal of attention from the liquid crystal research community and beyond. Experiments on generating umbilics (as conducted here) in a liquid crystal with positive dielectric anisotropy are extremely rare and the studies conducted were therefore also important to learn about the properties of umbilics in general.

Samples were made with an iron doped lithium niobate (Fe:LN) substrate and an ITO coated glass plate (additionally coated with a lecithin alignment layer) as covering substrate. Umbilics were created upon exposure with a focused laser beam: They were induced via photo generated fields at the relocatable exposure beam position. The field distribution of these photo generated fields is normal to the sample plane at the exposure spot center and has increasingly high in-plane field components in radial direction: Ideal conditions to induce director reorientations with radial symmetry in a liquid crystal with positive dielectric anisotropy. The irradiated regions were studied with polarized probe light revealing the characteristic patterns seen in umbilic defects and the typical doughnut-shaped intensity distributions expected for optical vortex beams.

The experimental findings were compared to calculated transmission profiles based on adjusted models (analytical models) of umbilics from literature.

The umbilics observed were relocated easily within the sample plane to any wanted position, which presented an exciting possibility to create optical vortex beams on purpose by the use of a steered focused laser beam (as writing or control light). Please see the attached publication [3] for figures and further explanations.

e-mail: alexander.lorenz@online.ms · cell phone: +49 177 305 13 24

6. Investigating samples and substrates

6.1. Samples made with different orientation of z-cut substrates

First experiments with the new setup revealed that the size of laser induced defects (Fig. 9) depended on whether the LC layer had been placed on the *+c* or *-c* surface of the Fe:LN substrate. These experiments were performed between crossed polarizers using test cells assembled with a Fe:LN substrate and a thin cover glass separated by 12 μm spacers and filled with the nematic liquid crystal MLC-2087. The samples were exposed to a collimated laser beam (520 nm, 50 mW) with a beam waist of approximately 20 μm, which led to a one-ring pattern in Fig. 9 A and a three-ring pattern in Fig. 9 B.

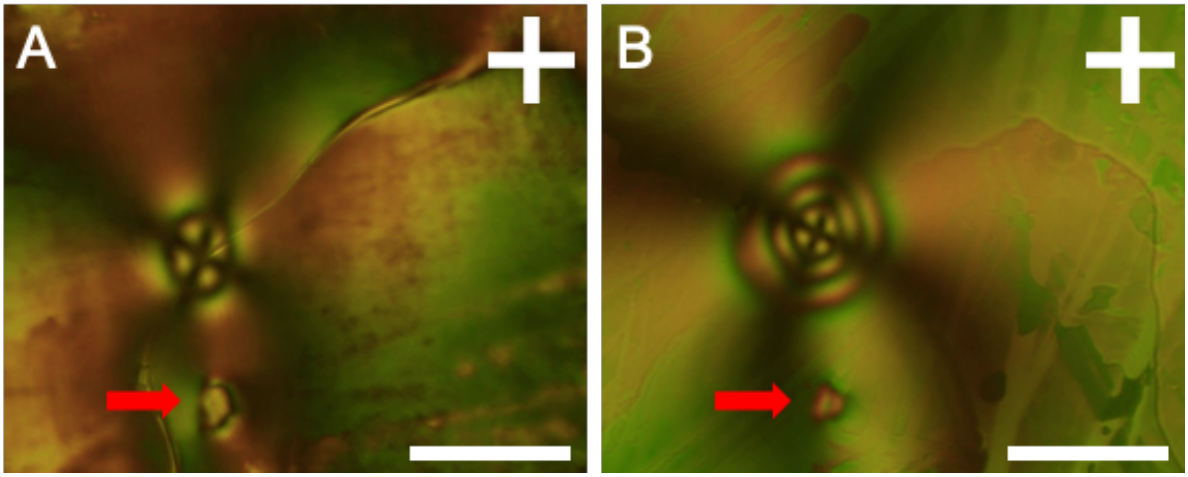

Fig. 9. Laser-induced defects on the *-c* (A) and *+c* (B) surface of a Fe:LN substrate observed between crossed polarizers. An additional laser spot with lower intensity, marked with a red arrow, appears because of the beam profile. The scalebar represents 100 μm.

The experimental setup with fixed beam alignment led to very reproducible exposure conditions: In both figures, a local director realignment caused by a secondary exposure spot (caused by surface reflections of optical elements used for beam shaping) can be seen (Fig. 9 A and B, marked with red arrows). The focal plane was investigated with a beam profiler (Fig. 10). As seen in the figure, the secondary exposure spot had much lower power density and appeared in a distance of 120 μm from the main exposure spot. Since the exposure condition were perfectly fixed by the setup, the reasons for the differences in the size of the defects needed to be further investigated. Contact angle (CA) measurements of the *+c* and *-c* surfaces of the substrates were conducted on each side of cleaned Fe:LN substrates to determine their surface energies and variations in their surface energies.

e-mail: alexander.lorenz@online.ms · cell phone: +49 177 305 13 24

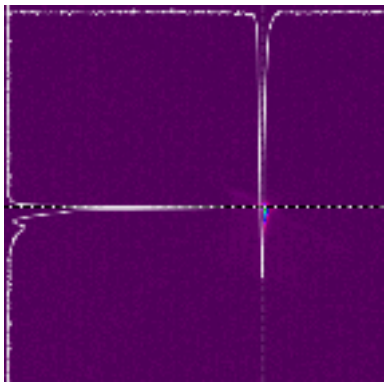

Fig. 10. The beam profile of the laser source (520 nm, 50 mW) shows perfect collimation in one direction, while an additional peak with much lower intensity cannot be avoided in the other direction.

6.2. Contact angle measurements

Already in an initial hand-experiment (a quick test with water as solvent), the contact angles measured on the *+c* and *-c* surface deviated by approx. 10°, supporting the idea of different surface properties. Therefore, a detailed study was conducted. The contact angles of 9 different test liquids were investigated using the static sessile drop method. A droplet of the test liquid was deposited on a cleaned Fe:LN surface and image sequences were recorded. Each measurement was repeated at least 3 times at different locations on the surface. The recorded images were analyzed and the initial contact angles as well as the equilibrium contact angles for the different liquids were determined. The impact of pre-illumination was also investigated (non-pre-illuminated vs. pre-illuminated samples). The results for non-pre-illuminated samples are shown in Fig. 11 for the *+c* and Fig. 12 for the *-c* surface.

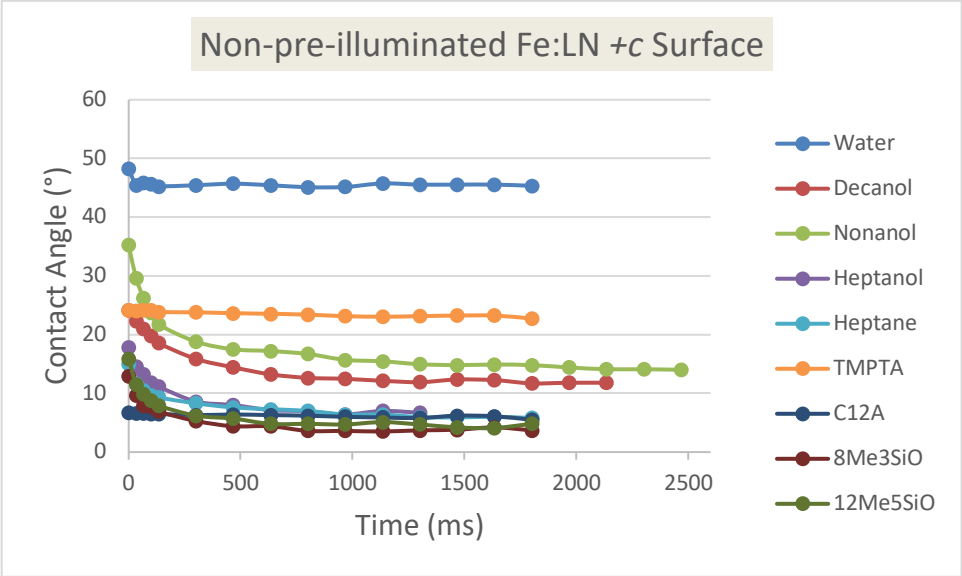

Fig. 11. Time dependent evaluation of contact angles on the *+c* surface for various liquids.

e-mail: alexander.lorenz@online.ms · cell phone: +49 177 305 13 24

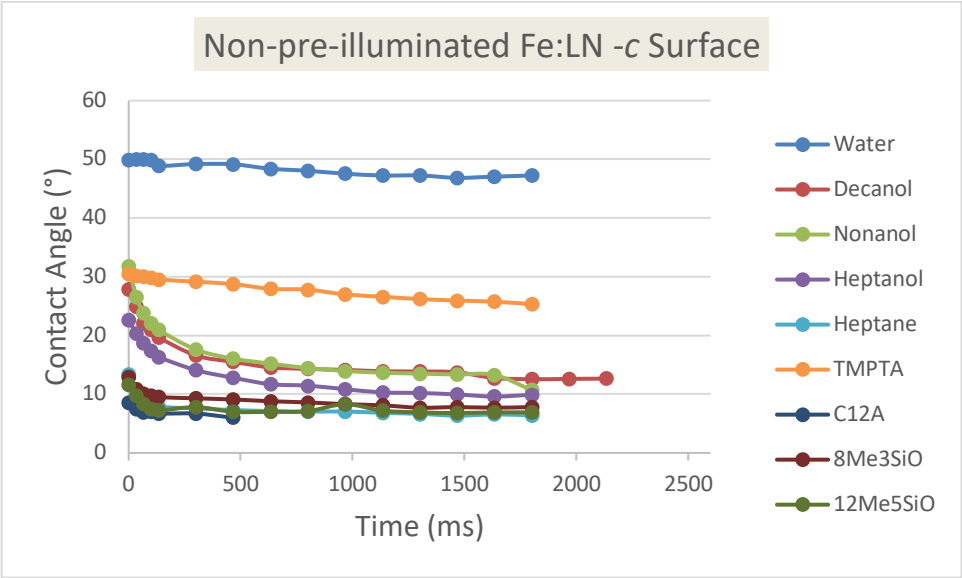

Fig. 12. Time dependent evaluation of contact angles on the *-c* surface for various liquids.

As shown in Fig. 11 and Fig. 12, a larger change of the contact angle was observed for some liquids directly after deposition of the droplet. This initial change results from spreading of the liquid on the substrate surface, which occurs during the first second after deposition of the droplet (before an equilibrium is established). Therefore, the contact angle measured after 1.5 s is referred to as equilibrium contact angle. Later changes of the contact angle can be attributed to evaporation effects, which result in a more or less linear decrease of the contact angle over time. Evaporation was a major issue only for the investigated siloxane compounds Octamethyl trisiloxane (8Me3SiO) and dodecamethyl pentasiloxane (12Me5SiO), where the solvent was completely evaporated after several seconds. Initial and equilibrium contact angles on the *+c* surface and *-c* surface of a non-pre-illuminated substrate are shown in Fig. 13 and Fig. 14, respectively. A summary is given in Fig. 15.

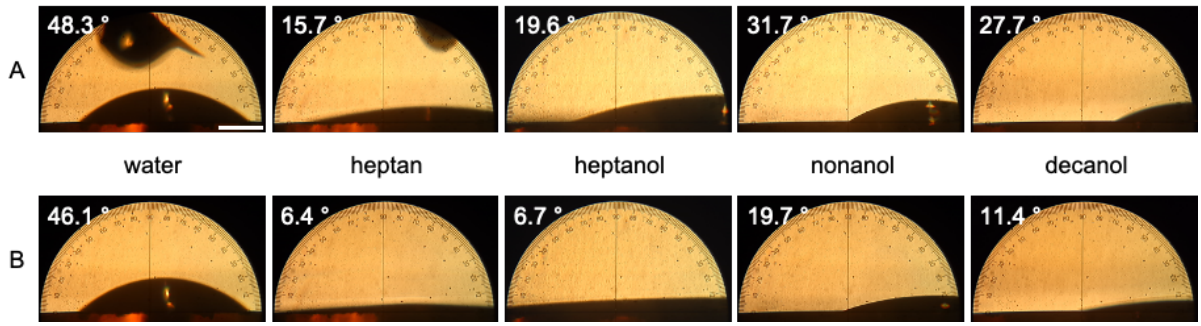

Fig. 13. The initial contact angle at t = 0 ms and the equilibrium contact angle at t = 1.5 s on the *+c* surface for several liquids are shown in A and B, respectively. The scalebar indicates a length of 200 μm.

e-mail: alexander.lorenz@online.ms · cell phone: +49 177 305 13 24

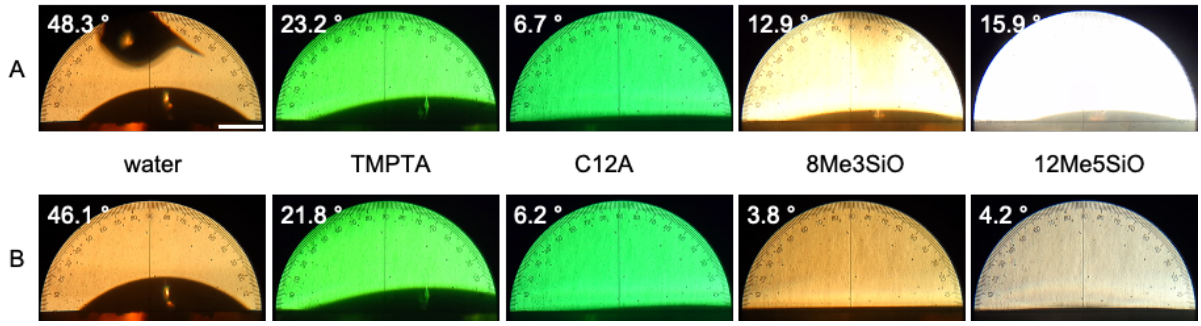

Fig. 14. Initial (A) and equilibrium (B) contact angles for water, the monomers trimethylolpropane triacylate (TMPTA) and dodecyl acrylate (C12A) and the two siloxanes 8Me3SiO and 12Me5SiO on the $+c$ surface are shown. To prevent polymerization, a green filter was used to investigate the monomers. The scalebar indicates a length of 200 μm.

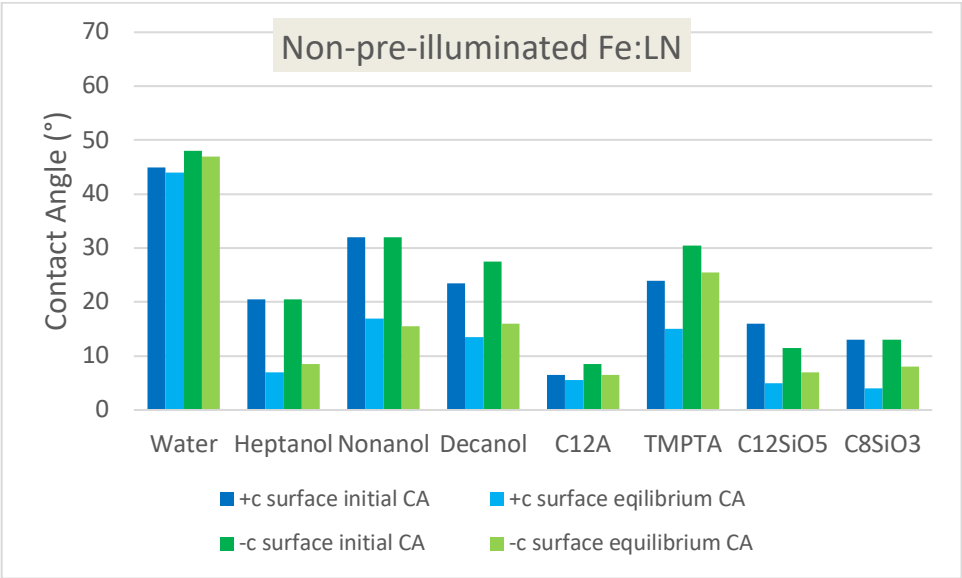

Fig. 15. Contact angles of various liquids on a non-pre-illuminated substrate.

This investigation also showed that typically contact angles on the $+c$ and $-c$ surface have similar values within the error range of the experiment (Fig. 15), which is in contradiction to the result from the first experiment. The passage of time since the last laser exposure experiment was conducted, was identified as the major difference between the first and later experiments. To assure that illumination causes these different contact angles, further investigation of pre-illuminated substrates was conducted. As it was difficult to achieve homogeneous illumination with a laser beam, white light LED illumination was used instead. To our surprise, exposing the substrate to white light for 2 h resulted in contact angle of water on the substrate (Fig. 16), which were similar to those observed in the first experiment.

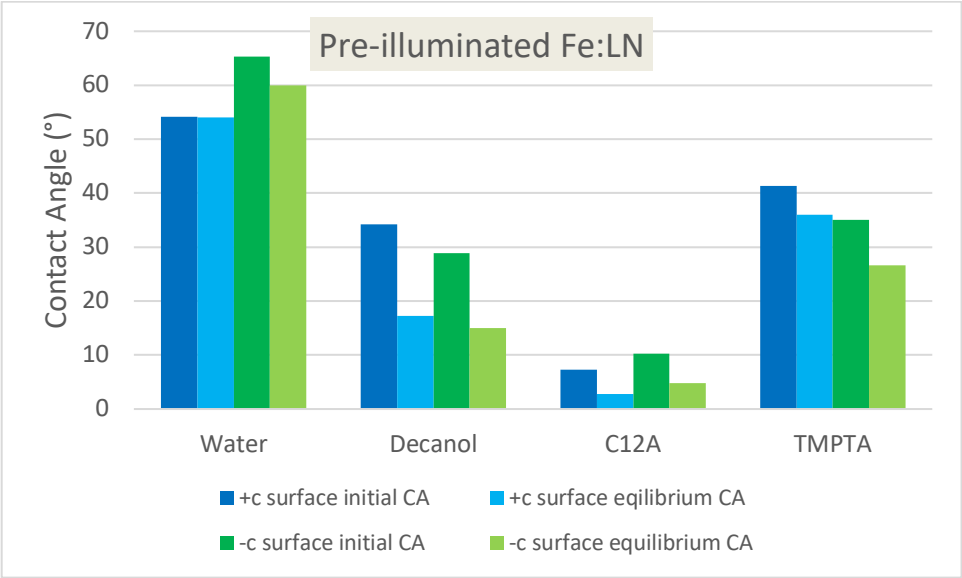

Fig. 16. Contact angles for selected liquids on an illuminated Fe:LN substrate.

In general, the contact angles of the investigated liquids are larger for illuminated than for non-pre-illuminated substrates on the *+c* and *-c* surface. However, this increase is not equal for both sides, but depends on the liquid; e.g. for water the contact angle on the *-c* surface increases more and on the *+c* surface increases less, while it is the other way round for TMPTA.

Using the Owen, Wendt, Rabel, and Kaelble (OWRK) method, the surface energy of the *+c* and *-c* surfaces of a non-pre-illuminated Fe:LN substrate was determined based on the initial or equilibrium contact angles.

6.3. Surface energy calculations

The OWRK method is a standard method for calculating the surface free energy of a solid substrate based on contact angles of probe liquids. The surface free energy of a solid γ_s, the surface tension of a liquid γ_l, and the interfacial energy γ_{sl} are related through Young's equation

$$\gamma_l \cos\theta = \gamma_s - \gamma_{sl}. \quad (1)$$

When the interactions between the two phases are interpreted as a geometric-mean of the dispersive γ^d and polar γ^p parts of the interfacial energy [R1]

$$\gamma_{sl} = \gamma_s + \gamma_l - 2\left(\sqrt{\gamma_s^d \gamma_l^d} + \sqrt{\gamma_s^p \gamma_l^p}\right), \quad (2)$$

substitution of γ_{sl} in Eq. (1) yields Eq. (3), which is displayed in a way most suitable to analyze the dispersive γ_s^d and polar γ_s^p parts of the substrate's surface free energy by linear regression.

$$\frac{\gamma_l(1+\cos\theta)}{2\sqrt{\gamma_l^d}} = \sqrt{\gamma_s^d} + \sqrt{\gamma_s^p}\sqrt{\frac{\gamma_l^p}{\gamma_l^d}} \quad (3)$$

e-mail: alexander.lorenz@online.ms · cell phone: +49 177 305 13 24

Another approach [R2] interprets the interactions as a harmonic-mean of the dispersive and polar parts of the interfacial energy. However, numerical calculations are required to solve Eq. (4).

$$\gamma_l\,(1+\cos\theta) = 4\left(\frac{\gamma_s^d\gamma_l^d}{\gamma_s^d+\gamma_l^d} + \frac{\gamma_s^p\gamma_l^p}{\gamma_s^p+\gamma_l^p}\right) \tag{4}$$

For the OWRK method, it is best practice to measure the contact angle of a polar and a non-polar liquid (distilled water and heptane in this study). In addition, contact angels of heptanol, nonanol, and decanol were investigated. These liquids were chosen because of their availability in combination with the existence of literature values for their polar and dispersive surface tension contributions.

Tab. 1. Literature [R3, R4] values of the dispersive and polar parts of the surface tension for the investigated liquids.

Substance	Dispersive	Polar	Surface Tension
Water [R3]	21.8	51	72.8
Decanol [R4]	26.49	1.83	28.32
Nonanol [R4]	32	2.06	27.84
Heptanol [R4]	25.19	1.46	26.65
Heptane [R3]	20.1	0	20.1

The analysis showed different dispersive and polar surface energy contributions depending on whether or not the contact angles of alcohols were included in the calculation. The summed-up surface energy remained at about 51 mN/m and if not considering the alcohols, the dispersive part was about 19 mN/m. If including the alcohols in the calculation a value of about 15 mN/m was found. Further investigations showed that this was related to the evaluation method (Fig. 17); the limit for perfect wetting of these alcohols as calculated by the geometric mean equation (Eq. (3)) is reached at a dispersive surface energy contribution of about 15 mN/m. In comparison, the limit for perfect wetting is only reached for a dispersive part of about 22 mN/m when calculating with the harmonic mean equation (Eq. (4)). No perfect wetting was observed of the studied alcohols. Anyway, the contact angles measured for these alcohols were rather small (< 10°), which indicates that the OWRK method is probably not suitable to fully evaluate the experiments: For contact angles < 10° the inaccuracy of the evaluation increases and for contact angles < 5° the distinction to perfect wetting becomes difficult, because value and error are of similar magnitude.

The results are nevertheless interesting and indicate that the harmonic mean equation need be solved numerically to calculate the surface energy of the substrates, which would be for future work.

e-mail: alexander.lorenz@online.ms · cell phone: +49 177 305 13 24

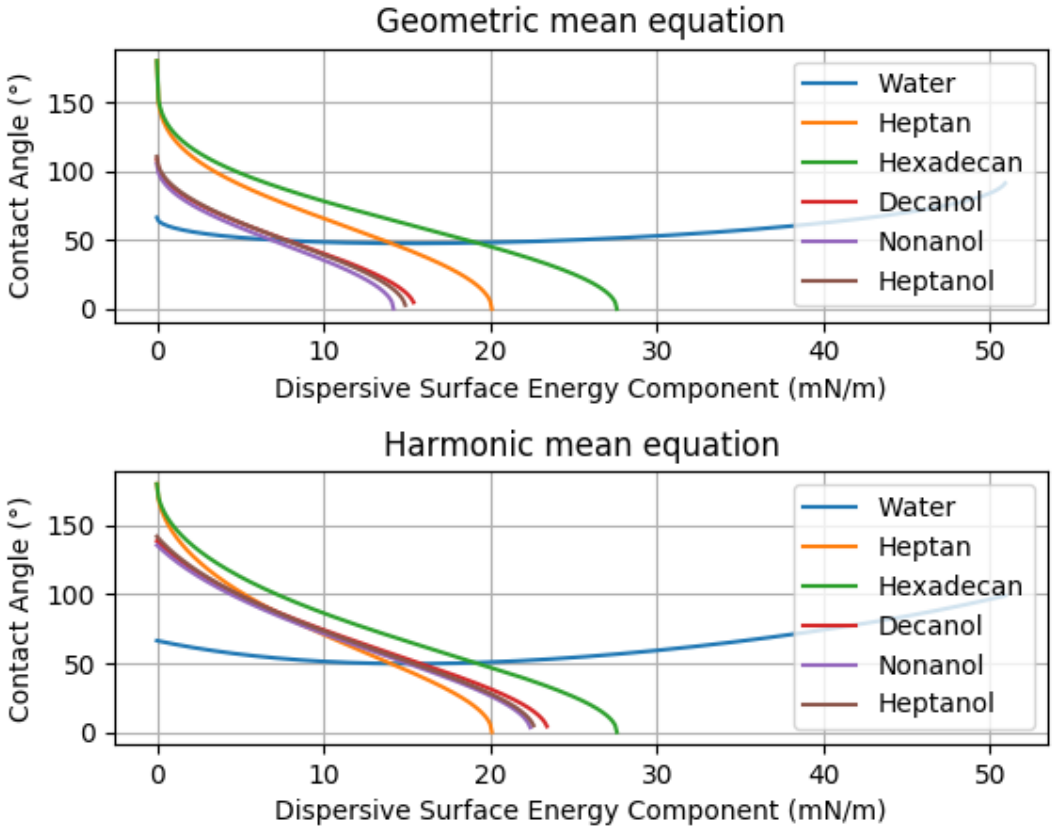

Fig. 17. Simulated change of the contact angle with variation of the dispersive surface energy component for a surface energy of 51 mN/m calculated based on the geometric or harmonic mean equation.

7. Summary, conclusions, outlook

The appearance of unwanted line defects in samples with chiral nematic LCs was efficiently avoided by surface treatment of the covering glass plate. In such samples, the defect size and the appearance (smooth defect edge) of light induced point like defects was controlled by surface treatment and by varying the exposure intensity and to a certain degree by use of lenses with various focal width.

Light valving in samples with a rather complex defect structure was studied in samples with *x*-cut iron doped lithium niobate substrates and initial vertical liquid crystal alignment. A comparison to the non-linear optical properties of the neat liquid crystal revealed that well-pronounced director realignments were achieved at light intensities several orders of magnitude lower than would be required in a neat liquid crystal driven without photovoltaic fields.

The new optical setup is promising to create patterns and reconfigurable gratings in our samples with higher precision than has been possible before.

We are currently studying samples with lecithin coated covering glasses, where the appearance (upon exposure) of line defects is suppressed. These samples are promising for the creation of (isolated: not connected to line defects) defects with radial symmetry (vortex

creation and potentially: optical trapping with controlled liquid crystal defects). Structured illumination and patterning are also being investigated.

Samples with indium tin oxide coated covering glasses, coated with lecithin as homeotropic alignment layer were efficiently used as canvas to create optical vortices in an isotropic background specifically at the exposure beam positing. In contrast to the previously explained experiments with a steered laser beam, samples were also investigated with a stationary and very stable exposure spot alignment. Here, the beam focus was fixed and it was intended to move the samples and write patterns. Surprisingly, it was revealed that the properties of the hybridized samples depended on the preconditioning of the light sensitive substrates and also on the orientation of their *c* axis. Samples with photovoltaic substrates coated with LC on their *+c* side showed a different behavior than was seen in samples where the LC was present on the *-c* surface. The contact angle of various test liquids was investigated when the liquid was placed selectively on the *+c* and *-c* surfaces of iron doped lithium niobate substrates, which were previously cleaned and annealed. Depending on the preconditioning (exposure to white light) the contact angle was found to vary. The investigations are challenging. However, it was found that a polar test liquid like water has a lower contact angle on the *+c* surface and this tendency is even more pronounced in a pre-illuminated substrate. Moreover, the difference between initial and equilibrium contact angles measured in non-polar solvents are slightly higher on the *+c* surface than on the *-c* surface in non-polar test liquids. Although such qualitative differences of the surface energies of *+c* and *-c* surface are clearly seen in the data, a quantitative analysis was not yet possible and would require more attention. A possible pathway is given in the presented data and discussions already.

e-mail: alexander.lorenz@online.ms · cell phone: +49 177 305 13 24

8. References

8.1. Publications

[1] S. Schafforz, Y. Yang, A. Lorenz, *Defect formation in N* LCs via photovoltaic fields: Impact of surface treatment*, Liq. Cryst., published online (2019). https://doi.org/10.1080/02678292.2019.1626923

[2] L. Jiao, D. R. Evans, A. Lorenz, *Photovoltaic light valve induced in a vertically aligned nematic liquid crystal on a x-cut Fe:LiNbO$_3$ substrate*, Journal Optical Data Processing and Storage (Special Issue: Photosensitive Soft Materials and Devices - Fundamentals and Applications, edited by A. Kiraz and L. Lucchetti) **4**, 8 (2018). https://doi.org/10.1515/odps-2018-0002

[3] S. L. Schafforz, G. Nordendorf, G. Nava, L. Lucchetti, A. Lorenz, *Formation of relocatable umbilical defects in a liquid crystal with positive dielectric anisotropy induced via photovoltaic fields*, J. Mol. Liq. 307, 112963 (2020). https://doi.org/10.1016/j.molliq.2020.112963

8.2. Conference presentations (oral presentations)

[O1] A. Lorenz, *Photovoltaic tweezers for optical manipulation in liquid crystals and dielectric fluids*, Bunsentagung 2019, Jena (May 30 – June 1, 2019).

[O2] A. Habibpourmoghadam, A. Lorenz, *Simulations of localized defect formation in hybridized LC test cells addressed via photovoltaic fields*, 46th German Liquid Crystal Conference, Paderborn (March 27 – 29, 2019).

[O3] **Keynote Presentation:** A. Lorenz, *Manipulating liquid crystals via photo generated fields and tailored polymer*, 5th International Conference on Physical and Theoretical Chemistry, Edinburgh, Scotland (October 11 – 13, 2018). https://www.omicsonline.org/proceedings/manipulating-liquid-crystals-via-photo-generated-fields-and-tailored-polymer-97669.html

8.3. Literature

[R1] D.K. Owens, R.C. Wendt, *Estimation of the surface free energy of polymers*, Journal of Applied Polymer Science. 13 (1969) 1741–1747. https://doi.org/10.1002/app.1969.070130815.

[R2] S. Wu, *Polar and Nonpolar Interactions in Adhesion*, The Journal of Adhesion. 5 (1973) 39–55. https://doi.org/10.1080/00218467308078437.

[R3] *Surface Tension Components and Molecular Weight of Selected Liquids*, https://www.accudynetest.com/surface_tension_table.html (accessed February 25, 2020).

[R4] L. Hołysz, E. Chibowski, *Surface Tension Components of some Organic Liquids*, in: Physikalische Chemie - Physical Chemistry, Carl Hanser Verlag, München, 1988: pp. 337–339.

e-mail: alexander.lorenz@online.ms · cell phone: +49 177 305 13 24

9. Lists

9.1. List of symbols, abbreviations, and acronyms

Contact angle (CA).

Dodecamethyl pentasiloxane (12Me5SiO).

Dodecyl acrylate (C12A).

Indium thin oxide (ITO).

Iron doped lithium niobate (Fe:LN).

Light emitting diode (LED).

Liquid crystal (LC).

Octamethyl trisiloxane (8Me3SiO).

Owen, Wendt, Rabel, and Kaelble (OWRK).

Photo voltaic (PV).

Trimethylolpropane triacylate (TMPTA).

9.2. List of figures

e-mail: alexander.lorenz@online.ms · cell phone: +49 177 305 13 24

9.3. List of Tables